S1 Methodology

S1.1   Scanning electron microscopy (SEM)

Backscattered electron (BSE, atomic Z-contrast) analysis was performed using an FEI Quanta 200F scanning electron microscope equipped with a field emission gun at the Scientific Center for Optical and Electron Microscopy (ScopeM) at ETH, Zurich. BSE settings were: acceleration voltage 10-20 kV, working distance 10 mm, aperture 3-4, spot size 4 and high vacuum. Thin sections were carbon-coated.

S1.2   γ-ray spectrometry (^{232}Th)

Trace concentrations of thorium in felsic gneisses and granitoids have been measured using γ-ray spectrometry. This method, rather than laser ablation inductively coupled plasma mass spectrometry (LA-ICP-MS), was applied, because it does not require extensive sample preparation and represents a quick and efficient method of acquiring the desired element concentration.

Thorium-232 accounts for 100 % of the element's natural abundance (Berglund and Wieser, 2011). Therefore, a sample's thorium content was assessed by quantifying the activity of this particular radioactive thorium isotope. Thorium-232 was not measured directly because it is a pure α-emitter without photon emission (Fig. S1). However, due to the Mesoproterozoic age (ca. 1200 Ma) of the deformation event (Musgravian Orogeny) which produced the contrasting thorium concentrations in the hanging wall and footwall of the Woodroffe Thrust, all products of the thorium-232 decay series (Fig. S1) can be assumed to be in equilibrium (secular equilibrium in the thorium series is obtained after only 30 years). As a consequence, the activity of thorium-232 and all daughter isotopes is the same. Thus, the thorium concentration can be indirectly measured via the γ-decay of the shorter-lived radium-228. The five most important peaks related to the γ-decay of radium-228 are located at 77.1 keV, 238.6 keV, 338.4 keV, 583.2 keV, 911.1 keV in the energy spectrum (Fig. S2). Measurements were conducted on thin section chips (weights ranging between 14-42 g) using γ-ray spectrometers at the Paul Scherrer Institute (PSI) in Villigen, Switzerland with a default measurement time of two hours. If the aspired error (2 x standard deviation) of 10 % was achieved earlier (thorium-rich samples), the measurement was stopped, otherwise it was run overnight for up to 15 hours (thorium-poor samples). Results were weight-averaged, with the highest significance being attributed to the strongest peak at 238.6 keV, in order to obtain the activity of radium-228 normalized to sample weight (Bq/kg). Following up on the assumption that the activity of thorium-232 and radium-228 are the same, this value was divided by the specific activity of thorium-232 (4060 Bq/g; Eikenberg, 2002) in order to obtain the concentration of thorium-232. The detection limit was determined from the 238.6 keV peak of lead-212. All measurements were done assuming a three centimetre plane source as sample geometry. Due to the dependence of the detector efficiency on the geometry and especially the thickness of each thin section chip, a correction factor was applied. This correction factor is equal to the relative difference between the detector efficiency of each sample with respect to the three centimetre plane source. All thin section chips were grouped according to their geometry and thickness and for each group a representative sample was chosen and the correction factor determined using a Monte Carlo approach.
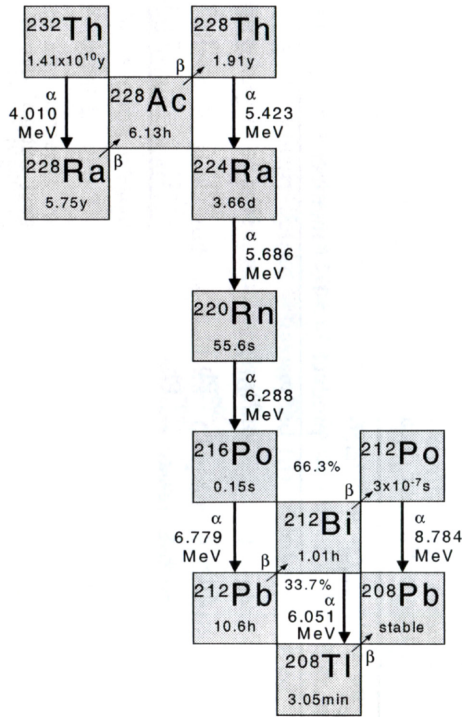
 Figure S1: Schematic illustration of the thorium-232 decay series members. For simplicity of the scheme, in comparison to standard isotope tables, neutrons are not considered. From Eikenberg (2002).
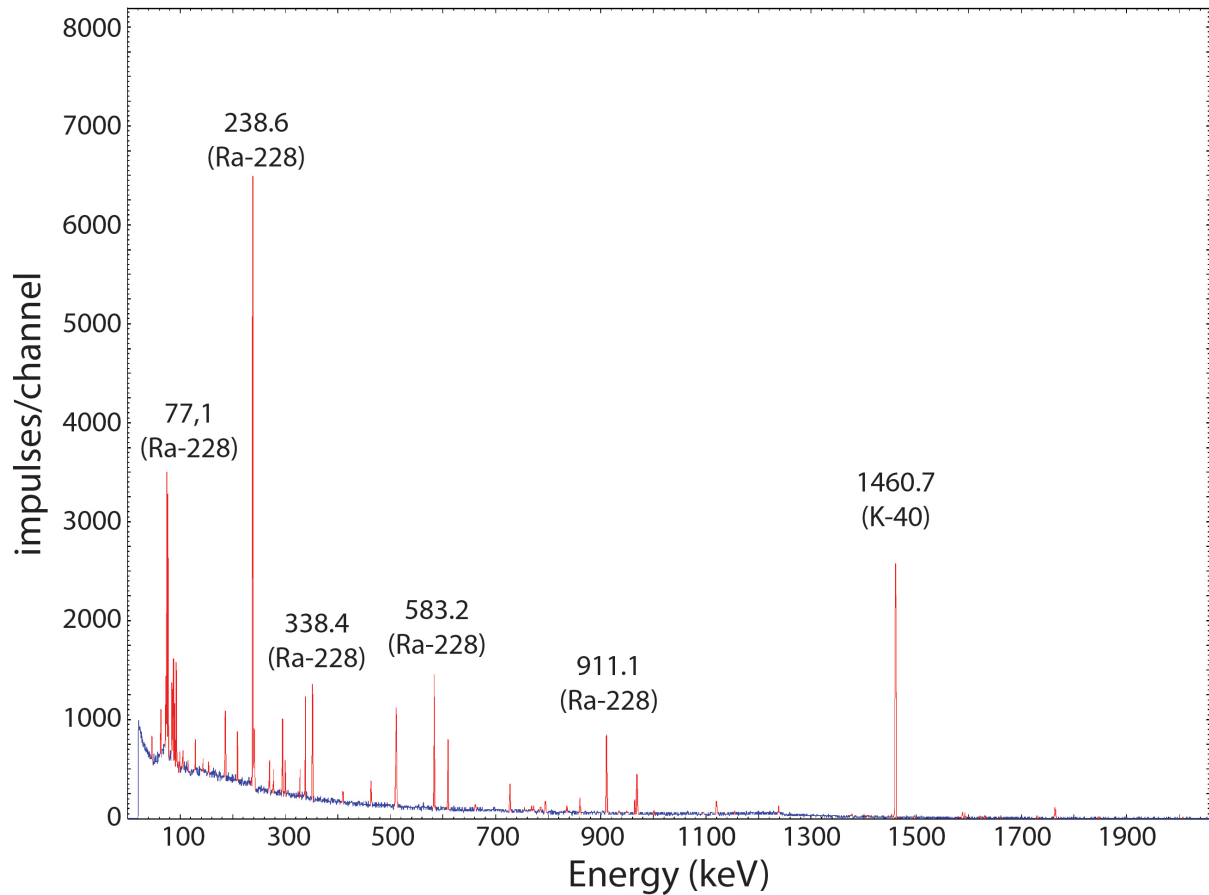
Figure S2: γ-spectrum of radium-228 with the most relevant energy peaks highlighted. Sample SW13-323A (coordinates: 132.14344, -25.99211; location 6 in Fig. 1 of the main paper).
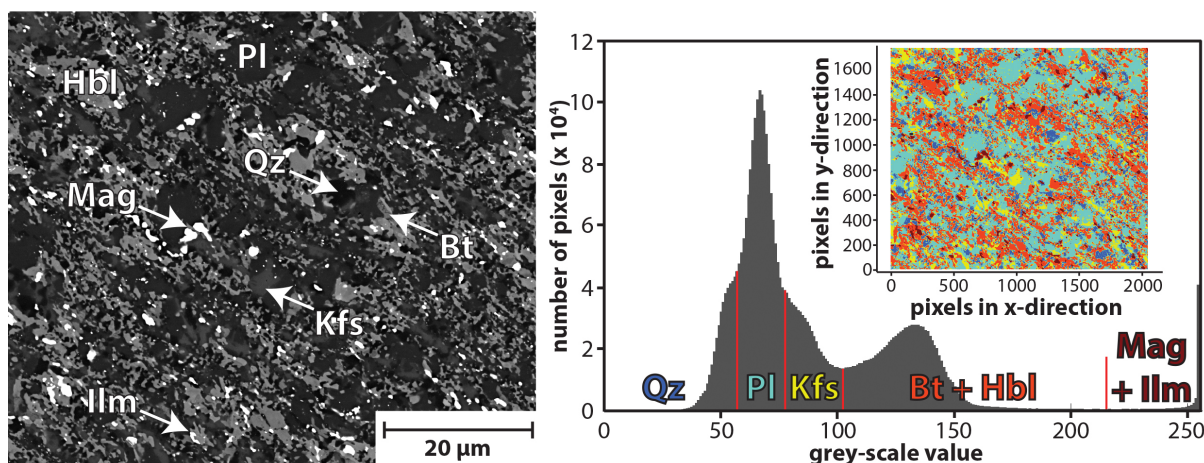
Figure S3: Calculation of the modal abundance of hydrous minerals from a BSE image. Thresholds (red lines) were set between the individual grey scale values ranges defined by each mineral. Thin section is not oriented. Sample FW13-093 (coordinates: 131.45213, -25.85455; location 3 in Fig. 1 of the main paper).

S1.3 Modal abundance of hydrous minerals

The modal abundance of hydrous minerals in thin section was quantified by running an image analysis script in Matlab R2013a (Fig. S3). Utilizing BSE images, thresholds were manually defined between the individual grey scale values ranges defined by each mineral. The modal abundance of each phase was calculated after subtracting all pixels that were not part of the stable mineral assemblage (e.g. holes and clasts in pseudotachylytes). The magnification was kept roughly constant at an image width between 60-80 μm.

S1.4 Calcite isotope analysis

Carbon ($\delta^{13}C_{Cal}$) and oxygen ($\delta^{18}O_{Cal}$) isotope analysis of fine-grained, syn-tectonically crystallized calcite has been performed using a GasBench II preparation device connected to a Delta V mass spectrometer (both ThermoFisher Scientific, Bremen) at the Geological Institute at ETH, Zurich. The analytical procedures follow Breitenbach and Bernasconi (2011). Due to the low concentrations of calcite, slight modifications to these procedures include an increase in the amount of analysed sample material (9-13 mg) and utilized orthophosphoric acid (eight droplets) as well as the use of larger vials (12 ml). The data are reported in the conventional delta notation with respect to the V-PDB (Vienna Pee Dee Belemnite) and V-SMOW (Vienna Standard Mean Ocean Water) standard. For a reliable signal the benchmark Amplitude 44 (Ampl 44) should be above 2000.

S1.5 Whole rock carbon isotope analysis

Whole rock carbon isotopy ($\delta^{13}C_{whole\ rock}$) was determined using a ThermoFisher Flash-EA 1112 coupled with a Conflo IV interface to a ThermoFisher Delta V isotope ratio mass spectrometer (IRMS). Samples were combusted in the presence of oxygen in an oxidation column at 1020 °C. Combustion gases are passed through a reduction column (650 °C), and produced nitrogen and carbon dioxide gases separated chromatographically and transferred to the IRMS via an open split for on-line isotope measurements. Isotope ratios are reported in the conventional delta notation with respect to the V-PDB (Vienna Pee Dee Belemnite) standard. The system is calibrated with NBS22 ($\delta^{13}C$ = -30.03 ‰) and IAEA CH-6 ($\delta^{13}C$ = -10.46 ‰). Reproducibility of the measurements is better than 0.2 ‰. For a reliable signal the benchmark Amplitude 44 (Ampl 44) should be above 2000.

S2 Calcite and whole rock stable isotopic signature

In an attempt to constrain the origin of the hydrothermally introduced carbon (Fig. 7c of the main paper), felsic and mafic samples, with and without fine-grained, syn-tectonically crystallized calcite, have been isotopically analysed (for details on the methods see Supporting Information S1), with the results for $\delta^{13}C_{Cal}$, $\delta^{18}O_{Cal}$, and $\delta^{13}C_{whole\ rock}$ summarized in Table S1. With the exception of SW13-173A, calcite isotopic signatures were obtained for all calcite-bearing samples, yielding $\delta^{13}C_{Cal}$ (V-PDB) values between -2.7 ‰ to -5.9 ‰ (mean average -4.1 ‰) and $\delta^{18}O_{Cal}$ (SMOW) values between +5.7 ‰ and +14.5 ‰ (mean average +10.1 ‰). Within the same samples, the $\delta^{13}C_{whole\ rock}$ (V-PDB) isotopic signature is always lower (on average by 2.7 ‰) than the corresponding $\delta^{13}C_{Cal}$ values. Calcite-free samples yield significantly lower $\delta^{13}C_{whole\ rock}$ values between -10.7 ‰ and -22.6 ‰ (Table S1), with this carbon presumably coming from CO_2 contained in fluid inclusions. The amplitude (Ampl 44) of each measurement functions as a benchmark for the data's reliability. This parameter should typically be above 2000 for a measurement to be considered trustworthy. Consequently, $\delta^{13}C_{Cal}$ and $\delta^{18}O_{Cal}$ of SW13-159 and NW14-408 are well constrained, whereas the results for NW13-203, SW14-025 and SW13-124 are less reliable. The low benchmark values almost certainly reflect the very low modal abundance of calcite in the studied rocks (typically <1 %). Nevertheless, the determined values for each of the five samples are reproducible in different runs and are very similar to each other, which argues for their reliability.

	location (Fig. 1)	sample	lithology	coordinates (WGS 1984)	run	GasBench II				Combustion	
						$\delta^{13}C_{cal}$(‰) (V-PDB ± 2σ)	$\delta^{18}O_{cal}$(‰) (V-PDB ± 2σ)	(SMOW)	Ampl 44	$\delta^{13}C_{whole\ rock}$(‰) (V-PDB)	Ampl 44
calcite-bearing	9	NW13-203	granite	131.74318 -26.00442	1	-4.12 ± 0.15	-21.19 ± 0.23	9.02	686	-9.36	4235
					2	-4.12 ± 0.08	-21.34 ± 0.25	8.86	936		
					3	-4.47 ± 0.10	-23.30 ± 0.13	6.84	872		
					4	-4.08 ± 0.12	-23.56 ± 0.11	6.57	852		
	9	SW14-025	granite	131.73269 -26.01569	1	-4.11 ± 0.34	-24.37 ± 0.25	5.74	432	-6.54	7500
					2	-3.92 ± 0.05	-24.25 ± 0.23	5.86	667		
	10	NW14-408	dolerite	131.85345 -26.11036	1	-5.83 ± 0.05	-19.90 ± 0.15	10.34	2120	-6.83	8069
					2	-5.85 ± 0.10	-19.90 ± 0.08	10.35	3463		
	12	SW13-124	granite	131.87272 -26.20402	1	-3.72 ± 0.14	-18.33 ± 0.29	11.97	625	-6.50	6110
					2	-3.77 ± 0.12	-18.16 ± 0.04	12.14	1099		
	14	SW13-159	felsic gneiss	131.77375 -26.30666	1	-2.76 ± 0.07	-16.01 ± 0.16	14.36	1569	-4.88	5743
					2	-2.71 ± 0.07	-15.88 ± 0.04	14.49	2305		
	2	SW13-173A	felsic gneiss	131.45334 -25.84543	1	- -	- -	-	5313	-10.68	2353
					2	- -	- -	-	5312		
calcite-free	7	SW13-104	granite	131.63509 -25.94122	1	- -	- -	-	7153	-22.56	983
					2	- -	- -	-	7156		
	13	SW14-194	dolerite	131.82577 -26.24931	1	- -	- -	-	5297	-22.61	838
					2	- -	- -	-	5292		
	14	SW13-166	dolerite	131.77451 -26.30822	1	- -	- -	-	5304	-17.29	960
					2	- -	- -	-	5294		

Table S1: Calcite ($\delta^{13}C_{Cal}$, $\delta^{18}O_{Cal}$) and whole rock ($\delta^{13}C_{whole\ rock}$) stable isotope results for the central Musgrave Block.

$\delta^{13}C_{Cal}$ should provide information on the brine source, since there are no other carbon-bearing phases in the studied rocks (Collerson et al., 1972; Major, 1973; Major and Conor, 1993; Scrimgeour and Close, 1999). $\delta^{18}O_{Cal}$, on the other hand, should reflect the calcite crystallization temperatures. Our results are in agreement with the

95   range of $\delta^{18}O$ values for metamorphic waters (Taylor, 1997, his Fig. 6.4) and carbonates (Coplen et al., 2002, their Fig. 6) at temperatures of 500-600 °C, considering that the corresponding fluid phase should isotopically have been ca. 5-6 ‰ heavier than the crystallizing calcite (Chacko et al., 1991). Our $\delta^{13}C_{Cal}$ results strongly overlap with the typical range of values for a rock-buffered system within igneous and metamorphic rocks (Coplen et al., 2002, their Fig. 4). However, from Table S1 it is evident that $\delta^{13}C_{Cal}$ is never identical to $\delta^{13}C_{whole\ rock}$.

100   Consequently, full rock-buffering has not been achieved and it should be possible to place some constraints on the potential carbon source. The range of determined $\delta^{13}C_{Cal}$ values excludes a marine origin (Coplen et al., 2002, their Fig. 4), but is in agreement with a mantle (Deines, 2002; Javoy et al., 1986) or sedimentary source (Bitter Springs Formation; Hill et al., 2000). Within the underlying Amadeus Basin sediments, the most likely source would have been either the carbonate-bearing Bitter Springs Formation or its lateral equivalent the Pinyinna Beds

105   (Wells et al., 1970; Young et al., 2002). However, both units do not crop out in the study area and, as outlined in Sect. 8.3.1 of the main paper, the Amadeus Basin sediments were potentially only imbricated below the Kelly Hills klippe after shearing on the Woodroffe Thrust had largely ceased. Hence, the CO_2-dominated brines are likely mantle-derived.

S3 Hydrous minerals in felsic pseudotachylytes
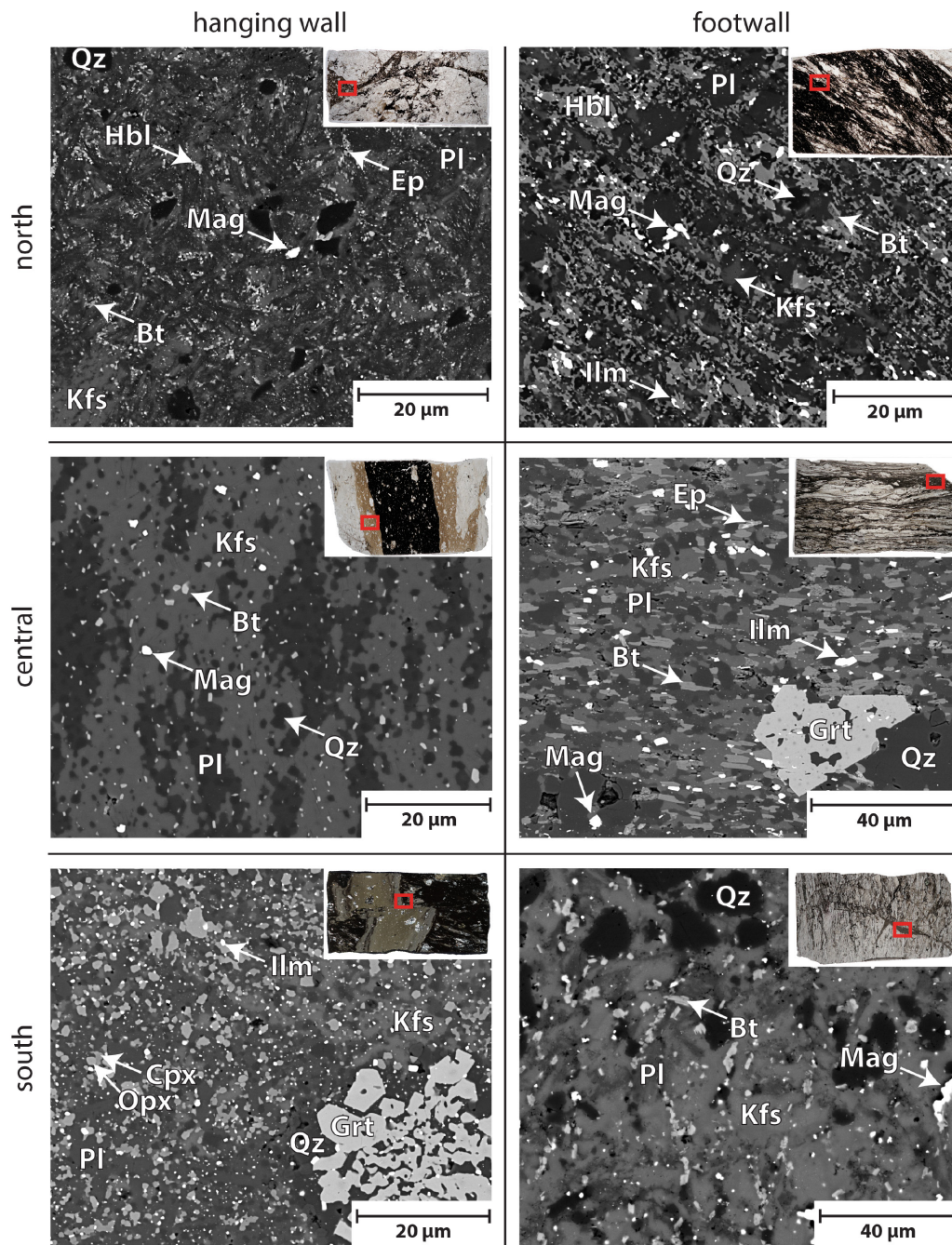
Figure S4: Representative BSE images of felsic pseudotachylytes from the hanging wall and footwall of the Woodroffe Thrust arranged into northern (locations 1-5 in Fig. 1 of the main paper), central (locations 6-9 in Fig. 1 of the main paper) and southern location groups (locations 11-14 in Fig. 1 of the main paper). Overview thin section images are roughly 4 cm in width. (top left) Unoriented sample FW13-096 (coordinates: 131.45034, -25.85414; location 3 in Fig. 1 of the main paper). (top right) Unoriented sample FW13-093 (coordinates: 131.45213, -25.85455; location 3 in Fig. 1 of the main paper). (centre left) Unoriented sample SW14-029A (coordinates: 131.74496, -26.00093; location 9 in Fig. 1 of the main paper). (centre right) Sample SW13-321 (coordinates: 132.14333, -25.99178; location 6 in Fig. 1 of the main paper). Thin section is oriented N-S (left-right). (bottom left) Loose sample SW14-181B (coordinates: 131.92595, -26.17664; location 11 in Fig. 1 of the main paper). (bottom right) Unoriented sample SW14-237C (coordinates: 131.83544, -26.25303; location 13 in Fig. 1 of the main paper).

S4 Plagioclase stability microstructure 3
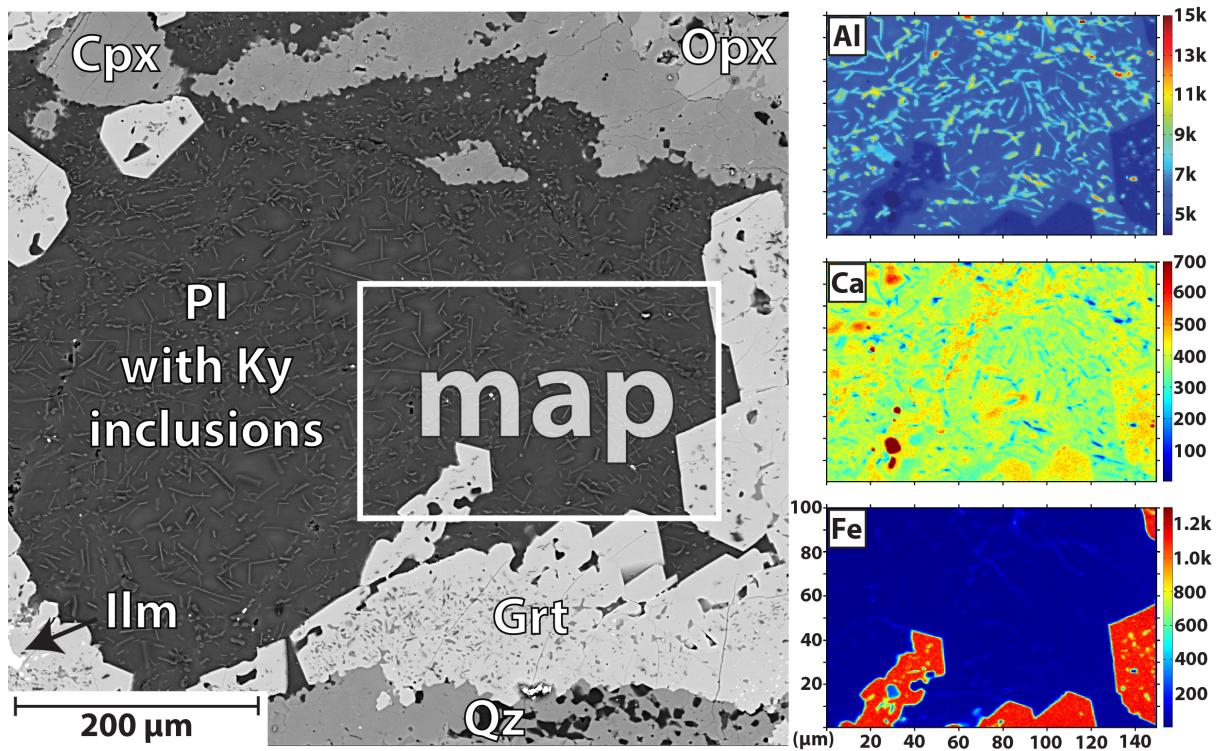
Figure S5: BSE image of plagioclase with kyanite inclusions (microstructure 3). Elemental maps (Al, Ca, Fe) do not indicate the presence of epidote. The host rock is a statically overprinted dolerite dyke with a stable mineral assemblage of Pl + Cpx + Grt + Ilm + Ky + Rt + Qz. Relict orthopyroxene is locally present (top right corner). Thin section is not oriented. Sample SW13-167 (coordinates: 131.77475, -26.30845; location 14 in Fig. 1 of the main paper).

125

S5 Local presence of free aqueous fluid
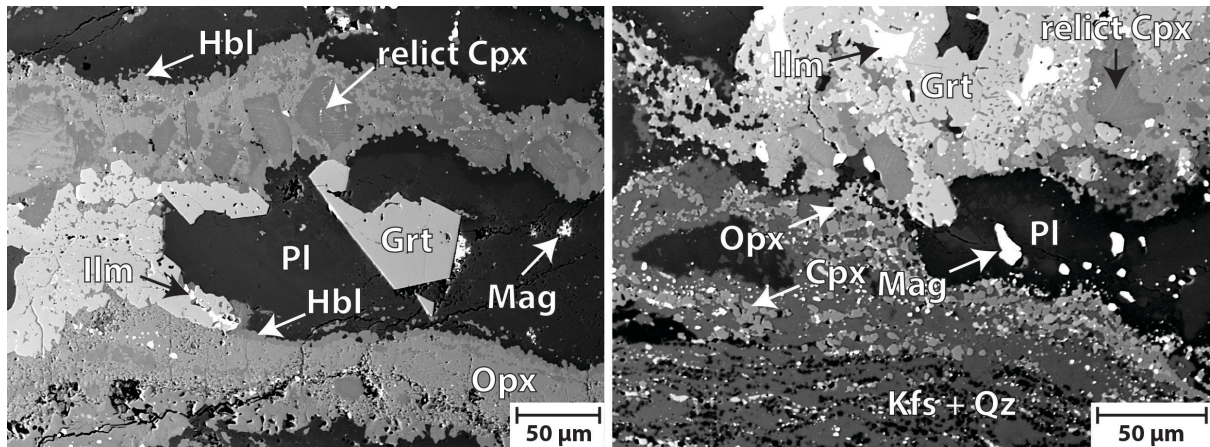
Figure S6: Sheared dolerite dyke from the footwall of the Woodroffe Thrust with two coevally developed mineral assemblages. Thin section is oriented N-S (left-right). Sample NW14-408 (coordinates: 131.85345, -26.11036; location 10 in Fig. 1 of the main paper). (left) Hydrous mineral assemblage Pl + Opx + Grt + Hbl + Ilm + Mag ± Cpx ± Bt. (right) Anhydrous mineral assemblage Pl + Opx + Grt + Cpx + Kfs + Qz + Ilm + Mag.

130